


## Revising the $H_2{}^{16}O$ line-shape parameters around 1.1 μm based on the speed-dependent Nelkin-Ghatak profile and the Hartmann-Tran profile

Hui Zhang(张惠), Jianjie Zheng(郑健捷), Qiang Liu(刘强), Wenyue Zhu(朱文越), Xianmei Qian(钱仙妹), Guisheng Jiang(江贵生), Shenlong Zha(查申龙), Qilei Zhang(张启磊), and Hongliang Ma(马宏亮)
**Citation:**Chin. Phys. B, 2023, 32 (**12**): 123301. DOI: 10.1088/1674-1056/acc7f5
Journal homepage: http://cpb.iphy.ac.cn; http://iopscience.iop.org/cpb

**What follows is a list of articles you may be interested in**

---

## Terahertz spectroscopy and lattice vibrational analysis of pararealgar and orpiment

Ya-Wei Zhang(张亚伟), Guan-Hua Ren(任冠华), Xiao-Qiang Su(苏晓强), Tian-Hua Meng(孟田华), and Guo-Zhong Zhao(赵国忠)
Chin. Phys. B, 2022, 31 (**10**): 103302. DOI: 10.1088/1674-1056/ac7cd3

## Computational design of ratiometric two-photon fluorescent $Zn^{2+}$ probes based on quinoline and di-2-picolylamine moieties

Zhe Shao(邵哲), Wen-Ying Zhang(张纹莹), and Ke Zhao(赵珂)
Chin. Phys. B, 2022, 31 (**5**): 053302. DOI: 10.1088/1674-1056/ac46c6

## Laser-induced fluorescence experimental spectroscopy and theoretical calculations of uranium monoxide

Xi-Lin Bai(白西林), Xue-Dong Zhang(张雪东), Fu-Qiang Zhang(张富强), and Timothy C Steimle
Chin. Phys. B, 2022, 31 (**5**): 053301. DOI: 10.1088/1674-1056/ac43a4

## Line positions, intensities, and Einstein *A* coefficients for 3-0 band of $^{12}C^{16}O$: A spectroscopy learning method

Zhi-Xiang Fan(范志祥), Zhi-Zhang Ni(倪志樟), Jie-Jie He(贺洁洁), Yi-Fan Wang(王一凡), Qun-Chao Fan(樊群超), Jia Fu(付佳), Yong-Gen Xu(徐勇根), Hui-Dong Li(李会东), Jie Ma(马杰), and Feng Xie(谢锋)
Chin. Phys. B, 2021, 30 (**12**): 123301. DOI: 10.1088/1674-1056/ac3069

## Responsive mechanism and coordination mode effect of a bipyridine-based two-photon fluorescent probe for zinc ion

Han Zhang(张瀚), Zhe Shao(邵哲), Ke Zhao(赵珂)
Chin. Phys. B, 2020, 29 (**8**): 083304. DOI: 10.1088/1674-1056/aba9b9

---

# Revising the $H_2{}^{16}O$ line-shape parameters around 1.1 μm based on the speed-dependent Nelkin–Ghatak profile and the Hartmann–Tran profile

Hui Zhang(张惠)[1], Jianjie Zheng(郑健捷)[2,3], Qiang Liu(刘强)[2,3], Wenyue Zhu(朱文越)[2,3], Xianmei Qian(钱仙妹)[2,3], Guisheng Jiang(江贵生)[1], Shenlong Zha(查申龙)[1], Qilei Zhang(张启磊)[1], and Hongliang Ma(马宏亮)[1,†]

[1] *School of Electrical Engineering and Intelligent Manufacturing, Anqing Normal University, Anqing* 246133, *China*
[2] *Key Laboratory of Atmospheric Optics, Anhui Institute of Optics and Fine Mechanics, HFIPS, Chinese Academy of Sciences, Hefei* 230031, *China*
[3] *Advanced Laser Technology Laboratory of Anhui Province, Hefei* 230037, *China*

(Received 21 October 2022; revised manuscript received 14 March 2023; accepted manuscript online 28 March 2023)

Accurate spectroscopic data for $H_2{}^{16}O$ in the 1.1 μm region are particularly important for the study of Earth's atmosphere. The pure water vapor molecular spectra were measured based on direct laser absorption spectroscopy using a narrow line-width external cavity diode laser combined with a high-precision Fabry–Pérot etalon. A total of 31 $H_2{}^{16}O$ transitions were studied for the first time by using the speed-dependent Nelkin–Ghatak profile and the Hartmann–Tran profile. From an accurate line-shape analysis, we obtained the line intensities and the self-broadening coefficients, and they are compared with the available data reported in the HITRAN 2016 database and the HITRAN 2020 database. Finally, we obtained information on the influence of Dicke narrowing, as well as the correlations between Dicke narrowing and speed dependence, and of speed-dependent effects.

**Keywords:** pure water vapor molecule, the speed-dependent Nelkin–Ghatak profile, the Hartmann–Tran profile, line intensities

**PACS:** 33.20.–t, 33.20.Ea **DOI:** 10.1088/1674-1056/acc7f5

## 1. Introduction

In the Earth's atmosphere, the pure water vapor molecule ($H_2{}^{16}O$) is the principal atmospheric absorber of infrared (IR) radiation with many strong absorption bands ranging from the microwave to the visible portions of the spectrum.[1] Among these bands are the window regions with much weaker absorption.[2] The analysis of $H_2{}^{16}O$ weak absorption characteristics in the atmospheric transmission window is of great significance for the study of atmospheric optics. Indeed, 1.1 μm is one of the important atmospheric transmission windows that are of key importance for various fields of science and technology, such as remote sensing of the atmosphere,[3] atmospheric absorption simulation,[4] and reliable quantitative studies of laser atmospheric transmission.[5] To fulfill the requirements of these important applications, precise line parameters (i.e., positions, intensities, and broadening coefficients) of the $H_2{}^{16}O$ spectral lines are required.

Currently, the HITRAN molecular spectroscopic database[6] is a prime resource for the reference spectroscopic data for $H_2{}^{16}O$ at 1.1 μm for atmospheric applications. However, the new edition of the HITRAN 2020 database can only provide Voigt profile (VP) parameters. Additionally, due to the importance of $H_2{}^{16}O$ spectral parameters in this region, the region has been extensively studied by many groups. Previously, the line parameters of $H_2{}^{16}O$ around 1.1 μm were studied by Regalia *et al.*,[7] Oudot *et al.*,[8] and Schermaul *et al.*,[9] but all the studies were also performed with the VP. For a long time, the VP accounting for pressure/collision and Doppler broadening has been the standard for the high-resolution line-by-line modeling of IR molecular absorption due to its simplicity and its fast computation time. However, with the ever-increasing sensitivity and accuracy of measurement techniques, the non-Voigt line-shapes that consider more physical effects should be introduced for the correct fit of the experiments.[10–12] To the best knowledge of the authors, for the $H_2{}^{16}O$ spectrum around 1.1 μm, only Zheng *et al.*[13] have reported the line-shape parameters fitted by the quadratic speed-dependent Voigt profile (qSDVP). Therefore, further research on $H_2{}^{16}O$ spectra with more refined profiles is needed for 1.1 μm.

Using a narrow line-width external cavity diode laser combined with a high-precision Fabry–Pérot etalon, we recently measured 31 spectral lines of $H_2{}^{16}O$ near the 1.1 μm band based on direct laser absorption spectroscopy.[13] A multi-spectrum fitting (MSF) program was used in conjunction with the qSDVP and the VP to extract the line parameters. This work is the continuation of a series devoted to the systematic study of the absorption spectrum of $H_2{}^{16}O$ around 1.1 μm

†Corresponding author. E-mail: hlgnma@foxmail.com
© 2023 Chinese Physical Society and IOP Publishing Ltd

by our group.[13,14] In this study, we revisit our analysis using the speed-dependent Nelkin–Ghatak profile (SDNGP) and the Hartmann–Tran profile (HTP) because of their more physically realistic properties.

The organization of this paper is as follows. Section 2 introduces the experimental equipment and describes the HTP and SDNGP models used as well as the fitting quality. In Section 3, the fitting quality for the HTP, SDNGP, speed-dependent Voigt profile (SDVP), and VP is compared. Next, the uncertainty of the line intensity and self-broadening are analyzed. Then, the line intensities and the self-broadening coefficients obtained in this work are compared with the values in the HITRAN 2016 database and HITRAN 2020 database, and the correlation between the self-broadening coefficients and the rotation frequency is observed. Finally, the Dicke narrowing effect, the speed-dependent broadening, and the correlation between them are discussed.

## 2. Experimental setup and basic principles

### 2.1. Experimental setup

The experimental equipment used for data collection is described in detail in Ref. [13], so it is only briefly discussed here. As shown in Fig. 1, the external cavity diode laser (ECDL) is selected as the laser source in this device, and the wavelength coverage of the laser is from 9090 $cm^{-1}$ to 9750 $cm^{-1}$. The output laser light source is divided into two parts. One light source enters the gas absorption cell (which can provide a long optical path of 7246 cm and a short optical path of 3623 cm) for optical path absorption, and the other light source enters the Fabry–Pérot cavity for relative wavenumber calibration (the FSR of the Fabry–Pérot etalon is 750 MHz and the resolution is 1.2 MHz). Because near-infrared light is invisible, a He–Ne laser is used for optical path tracking. Finally, a data acquisition card controlled by the LabVIEW program receives the signal detected by the detector.

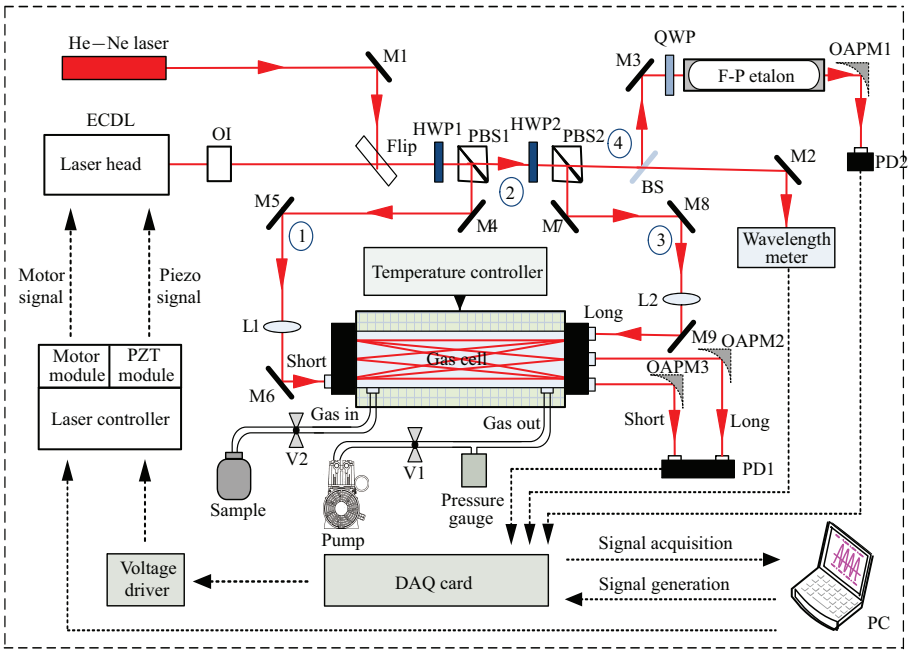



**Fig. 1.** Experimental apparatus for spectral measurement.

To obtain a high signal-to-noise ratio, the long optical path (7246 cm) of the gas absorption cell was selected in the experiment. The temperature was controlled at approximately 300 K in the process of data acquisition. Spectral data were measured at the three pressures of 1400 Pa, 1800 Pa, and 2000 Pa. Five sets of data were measured for each spectral line at the three pressures. In the process of pressure stabilization, the water vapor in the cell is filled and emptied many times. The purpose is to ensure that the water is absorbed by the cavity wall of the cell until the cavity wall is close to the saturation point and can no longer absorb water vapor easily. In this way, the experimental error caused by pressure fluctuation caused by water adsorption can be reduced.

### 2.2. Line-shape models

The HTP model is described as the partially correlated quadratic-speed-dependent hard-collision profile (pCqSDHCP).[15] The model is represented as

$$I_{\mathrm{HTP}}(\nu)=\frac{1}{\pi}\mathrm{Re}\left\{\frac{A(\nu)}{1-[\nu_{\mathrm{VC}}-\eta(C_0-3C_2/2)]A(\nu)+\left(\eta C_2/\nu_{\mathrm{a0}}^2\right)B(\nu)}\right\}. \tag{1}$$

The terms $A(v)$ and $B(v)$ depend on the complex probability function

$$w(z) = \frac{\mathrm{i}}{\pi}\int_{-\infty}^{+\infty}\frac{\mathrm{e}^{-t^2}}{z-t}\,\mathrm{d}t = \mathrm{e}^{-z^2}\mathrm{erfc}(-\mathrm{i}z), \tag{2}$$

where erfc is the Gauss error function. Therefore,

$$A(v) = \frac{\sqrt{\pi}c}{v_0 v_{\mathrm{a0}}}\left[w(\mathrm{i}Z_-) - w(\mathrm{i}Z_+)\right], \tag{3}$$

$$B(v) = \frac{v_{\mathrm{a0}}^2}{\tilde{C}_2}\left[-1 + \frac{\sqrt{\pi}}{2\sqrt{Y}}\left(1-Z_-^2\right)w(\mathrm{i}Z_-) - \frac{\sqrt{\pi}}{2\sqrt{Y}}\left(1-Z_+^2\right)w(\mathrm{i}Z_+)\right], \tag{4}$$

where

$$Z_\pm = \sqrt{X+Y} \pm \sqrt{Y}, \tag{5}$$

$$X = \frac{-\mathrm{i}(v_0 - v) + \tilde{C}_0}{\tilde{C}_2}, \tag{6}$$

$$Y = \left(\frac{v_0 v_{\mathrm{a0}}}{2c\tilde{C}_2}\right)^2. \tag{7}$$

In these expressions, $v_0$ is the most probable speed, and

$$\tilde{C}_0 = (1-\eta)\left(C_0 - \frac{3C_2}{2}\right) + v_{\mathrm{VC}}, \tag{8}$$

$$\tilde{C}_2 = (1-\eta)C_2, \tag{9}$$

$$C_n = \Gamma_n + \mathrm{i}\Delta_n, \tag{10}$$

$$v_{\mathrm{a0}} = \sqrt{\frac{2k_{\mathrm{B}}T}{M}} = \frac{c\Gamma_{\mathrm{D}}}{\sqrt{\ln(2)}\,v_0}. \tag{11}$$

This model fully considers the influence of multiple physical effects on spectral fitting.[16] It not only contains the Doppler broadening ($\Gamma_{\mathrm{D}}$), pressure shift ($\Delta_0$), and collision broadening ($\Gamma_0$) parameters of the VP but also includes the non-Voigt-effect parameters, such as the speed-dependent collision broadening coefficients ($\Gamma_2$), the speed-dependent shift coefficients ($\Delta_2$), and the Dicke narrowing coefficients ($v_{\mathrm{VC}}$). It also considers the relationship between the Dicke narrowing effect and the speed-dependent effect. The relationship is denoted by $\eta$.

The ratio of the speed-dependent broadening to the collisional broadening ($\alpha_{\mathrm{W}}$)[17] can be expressed as

$$\alpha_{\mathrm{W}} = \frac{\Gamma_2}{\Gamma_0} = (1-n)\frac{2}{3}\frac{m_{\mathrm{p}}/m_{\mathrm{a}}}{1+m_{\mathrm{p}}/m_{\mathrm{a}}}, \tag{12}$$

where $n$ is the temperature dependence coefficient and $m_{\mathrm{p}}/m_{\mathrm{a}}$ is the perturber-to-absorber mass ratio.

The $v_{\mathrm{VC}}$[18] can be expressed as

$$v_{\mathrm{VC}} = \frac{k_{\mathrm{B}}T}{2\pi c m D_{12}}, \tag{13}$$

where $k_{\mathrm{B}}$ is the Boltzmann constant, $c$ is the speed of light, $m$ is the $H_2O$ molecular mass, and $D_{12}$ is the mass diffusion coefficient, which can be calculated based solely on the molecular gas properties.[19] When $\eta = 0$, the modified model can be simplified to the SDNGP.[20]

### 2.3. The quality-of-fit

In addition to the SNR, the effect of spectral fitting can also be evaluated using the quality-of-fit (QF),[21] which is expressed as follows:

$$\mathrm{QF} = \frac{(\alpha_{\max} - \alpha_{\min})}{\tilde{S}_{\mathrm{R}}}, \tag{14}$$

where $\alpha_{\max} - \alpha_{\min}$ is the peak absorption signal and $\tilde{S}_{\mathrm{R}}$ is the standard deviation of the fitting residual. $\tilde{S}_{\mathrm{R}}$ is expressed as

$$\tilde{S}_{\mathrm{R}} = \sqrt{\frac{\sum_{i=1}^{M}a_{\exp}(v_i) - a_{\mathrm{fit}}(v_i)^2}{M - k_{\mathrm{p}}}}, \tag{15}$$

where $M$ is the number of measured spectral points, $k_{\mathrm{p}}$ is the number of adjustable parameters in multi-spectral fitting, $v_i$ is the first frequency of the measured spectrum, and $a_{\exp}(v_i)$ and $a_{\mathrm{fit}}(v_i)$ are the experimental and fitted absorption coefficients of the given spectral measurement points, respectively.

## 3. Results and discussion

### 3.1. Comparison of line-shapes

In this work, the measured data are reprocessed and then fitted with the multi-spectrum analysis tool for spectroscopy (MATS).[22] To better distinguish the fitting effects among different line-shapes, we test four line-shapes, which are the VP, SDVP, SDNGP, and HTP for spectrum fitting. Figure 2 displays an example of a spectrum recorded near 9129.21791 $\mathrm{cm}^{-1}$ for the fitting residuals of the HTP, SDNGP, SDVP, and VP for the same experimental conditions. As can be seen from Fig. 2, the residual values for the HTP, SDNGP, and SDVP are clinically almost indistinguishable but are all smaller than those determined with the VP. This is also similar to the situation mentioned in Ref. [15] in that the obvious residual with the VP is mainly caused by the line narrowing effect.

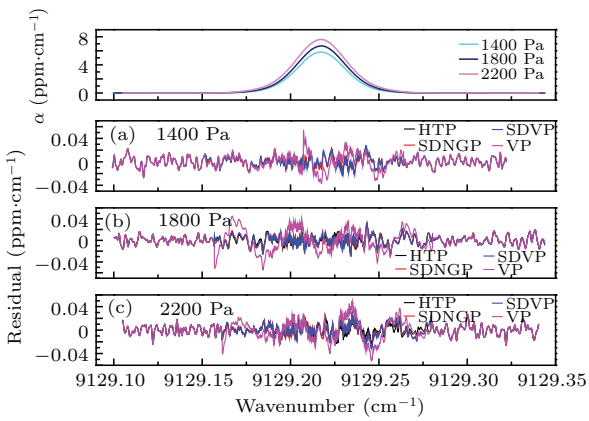



**Fig. 2.** Absorbance profiles fitted by HTP and the residuals for VP, SDVP, SDNGP, and HTP for the transition at 9129.21791 $\mathrm{cm}^{-1}$ in pure $H_2{}^{16}O$ at the pressures of 1400 Pa (a), 1800 Pa (b) and 2200 Pa (c).

To investigate the fitting effects of different line-shapes, the QF have been computed. In Fig. 3, we have noticed that: firstly, all the QF values increase with the pressure; secondly, $QF_{HTP} > QF_{SDNGP} > QF_{SDVP} > QF_{VP}$ was noticed from the dataset. Since the better results are obtained using the SDNGP and HTP, these two line-shapes were used for the following data processing.

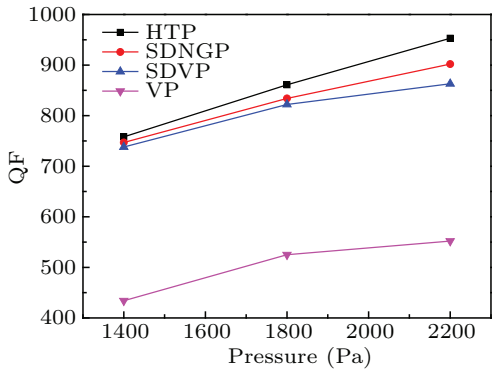



**Fig. 3.** The QF values as a function of the pressure at various profiles for the transition of 9129.21791 $cm^{-1}$ of $H_2{}^{16}O$.

### 3.2. Uncertainty analysis

The integral absorbance of the absorption line of a water molecule transition is

$$A = -\int_{-\infty}^{+\infty} \ln\left[\frac{I(\nu)}{I_0(\nu)}\right] d\nu = L\int_{-\infty}^{+\infty} N\sigma(\nu)\,d\nu$$
$$= NL\int_{-\infty}^{+\infty} S\phi_V(\nu)\,d\nu = NLS, \tag{16}$$

$$N = \frac{N_A \cdot P}{8.314472 \times 10^6 \cdot T}, \tag{17}$$

where $N$ (molecule·$cm^{-3}$) is the number concentration of water molecules, $L$ (cm) is the actual optical path of the absorption spectrum, $N_A$ is the Avogadro constant, and $P$ (Pa) is the pressure of water molecules. According to Eqs. (16) and (17), the line intensity of the absorption spectrum can be obtained as follows:

$$S = \frac{8.314472 \times 10^6 \cdot A \cdot T}{N_A \cdot P \cdot L}, \tag{18}$$

and from Eq. (18), the estimated uncertainties $\Delta P/P$, $\Delta L/L$, $\Delta T/T$, and $\Delta A/A$ can be combined in the usual way

$$\frac{\Delta S}{S} = \sqrt{\left(\frac{\Delta P}{P}\right)^2 + \left(\frac{\Delta L}{L}\right)^2 + \left(\frac{\Delta T}{T}\right)^2 + \left(\frac{\Delta A}{A}\right)^2}, \tag{19}$$

where $\Delta P/P = 1\%$ (due to the pressure gauge error and the adsorption of water), $\Delta L/L = 0.13\%$ (standard deviation obtained by averaging the optical path lengths of the inversion at different pressures), and $\Delta T/T = 0.1\%$ (the floating range is 0.3 K for the temperature of 300 K). The uncertainty $\Delta A/A$ is obtained with MATS software fitting (converting the error of the integral absorbance into the error of the line intensity). The values of $\Delta A/A$ from SDNGP-based fitting and HTP-based fitting are 2.50% and 3.27%, respectively. The comprehensive uncertainty estimates of the SDNP and HTP spectral line intensities obtained from Eq. (19) are 2.70% and 3.42%.

The total uncertainty of the self-broadening coefficient is calculated as follows:

$$\frac{\Delta\gamma_{self}}{\gamma_{self}} = \sqrt{\left(\frac{\Delta P}{P}\right)^2 + \left(\frac{\Delta\gamma_C}{\gamma_C}\right)^2 + \left(\frac{\Delta T}{T}\right)^2}, \tag{20}$$

where the uncertainty $\Delta P/P = 1\%$, $\Delta T/T = 0.1\%$, and $\Delta\gamma_C$ is the value of the collision broadening. The uncertainty $\Delta\gamma_C/\gamma_C$ is obtained with MATS software fitting (the error of collision broadening is converted into the error for the self-broadening coefficient). The values of $\Delta\gamma_C/\gamma_C$ from the SDNGP-based fitting and HTP-based fitting are 4.17% and 4.82%, respectively. According to Eq. (20), the total uncertainty estimates of the self-broadening coefficient are 4.29% (for the SDNGP) and 4.94% (for the HTP).

### 3.3. Line intensities analysis

In this work, thirty-one lines of $H_2{}^{16}O$ in the 9090–9750 $cm^{-1}$ region have been studied. All the parameters were converted to 296 K and 1 atm conditions.

In Figs. 4 and 5, the line intensities from our measurements were compared with those given in the HITRAN 2020 database and the HITRAN 2016 database, respectively. The percent differences (present work − other results)/(other results)×100% between our SDNGP results and the HITRAN 2020 values are shown in Fig. 4(a). Except for the lines of 9182.87814 $cm^{-1}$, 9731.64094 $cm^{-1}$, and 9734.20309 $cm^{-1}$, our line intensities are smaller than those of HITRAN 2020. The average percent difference between our results and HITRAN 2020 is −3.85%. Additionally, the percent differences between our HTP values and those from HITRAN 2020 are shown in Fig. 4(b). Similarly, the line intensities with HTP fitting are smaller than those of HITRAN 2020, except for the three absorption lines of 9323.18107 $cm^{-1}$, 9731.64094 $cm^{-1}$, and 9734.20309 $cm^{-1}$. The average percent difference between our HTP results and HITRAN 2020 is −3.71%. Overall, the HTP results of this work are close to the HITRAN 2020 values.

We also compared our work with the results in HITRAN 2016, and the percent differences are shown in Fig. 5. It can be noticed that the percent differences of these 31 absorption lines, whether for SDNGP-based fitting or HTP-based fitting, are evenly distributed on both sides of the axis 0. Additionally, the average percent differences between HITRAN 2016 and SDNGP-based fitting as well as HTP-based fitting are 2.61% and 2.40%. It should be noted that the HTP values are slightly larger than the SDNGP values.

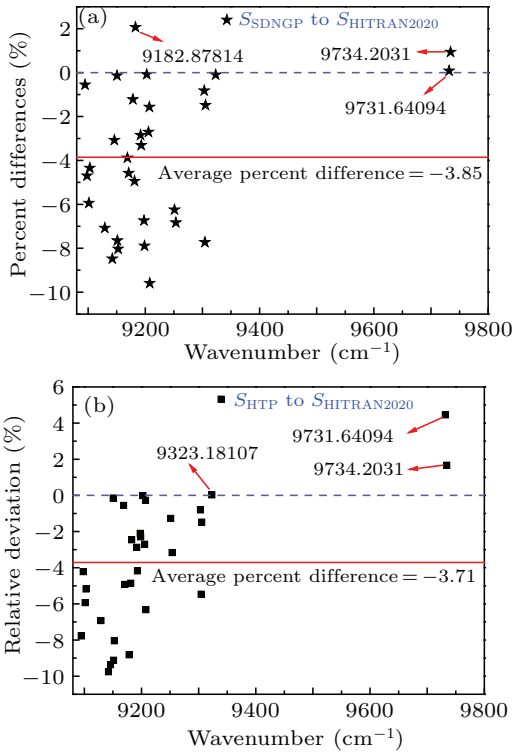



**Fig. 4.** The percent differences of the line intensities of the pure water vapor molecular lines obtained using the SDNGP (a) and the HTP (b) to those reported by HITRAN 2020.

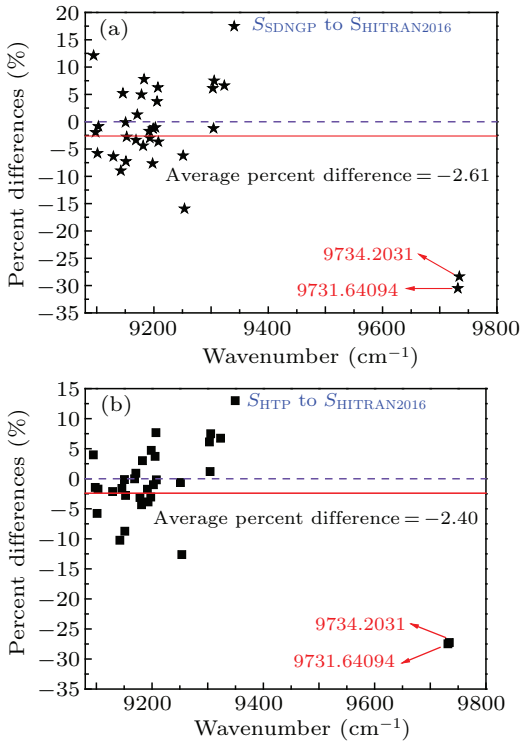



**Fig. 5.** The percent differences of the line intensities of the pure water vapor molecular lines obtained using the SDNGP (a) and the HTP (b) to those reported by HITRAN 2016.

For the two absorption lines of 9731.64094 cm$^{-1}$ and 9734.20309 cm$^{-1}$, our line intensities are obviously smaller than the HITRAN 2016 values. The percent differences are about −30.5% and −28.4% between our results by SDNGP fitting and those from HITRAN 2016, respectively. At the same time, the percent differences are about −27.5% and −27.3% between our results by HTP fitting and those from HITRAN 2016, respectively. It is worth mentioning that the line intensities of these two pure water vapor molecular lines have been updated in HITRAN 2020, and their values have changed greatly. The line intensities obtained with SDNGP fitting are slightly larger than those reported in HITRAN 2020 with average differences of 0.08% and 0.93%. Similarly, the percent differences for these two lines between our study by HTP fitting and the values in HITRAN 2020 are 4.45% and 1.67%, respectively.

### 3.4. Self-broadening coefficients analysis

The self-broadening coefficients for the SDNGP and HTP fitting from this study are presented in Fig. 6 and compared with the data from HITRAN 2020 (the self-broadening coefficients of these thirty-one water vapor absorption lines are consistent in HITRAN 2016 and HITRAN 2020). As shown in Fig. 6, the average percent differences between HITRAN 2020 and SDNGP-based fitting as well as HTP-based fitting are 2.70% and 3.26%. Most of the self-broadening coefficients of each spectral line that is fitted with the SDNGP and HTP in this work are larger than those provided by the HITRAN 2020 database. Note that the self-broadening coefficients of these lines from the HITRAN database are obtained using the VP. It is however worth mentioning that when using more refined models, several studies showed that the line broadening determined by the VP can be significantly underestimated.[23–27]

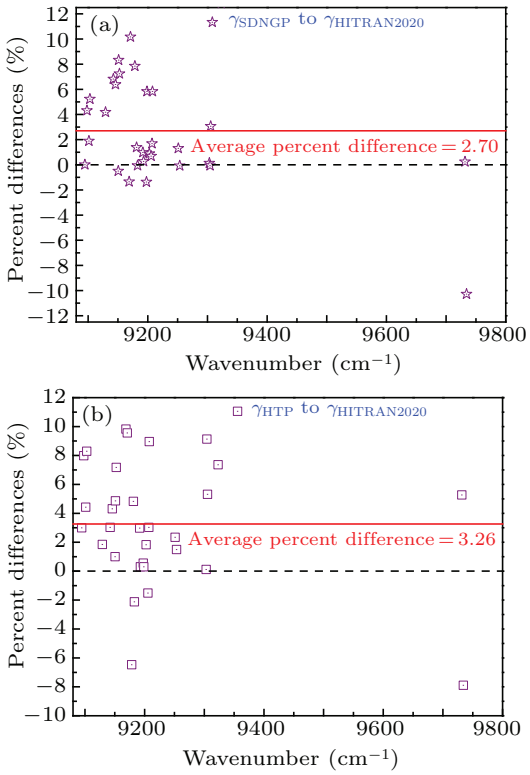



**Fig. 6.** The percent differences of the self-broadening coefficients of the pure water vapor molecular lines obtained using the SDNGP (a) and the HTP (b) to those reported by HITRAN 2020.

The relationship between the thirty-one absorption lines' self-broadening coefficients and rotational quantum number ($m$) are shown in Fig. 7. All the results present similar $m$-dependences. This indicates that the self-broadening coefficients of a water molecule has a good relationship with its rotation frequency.

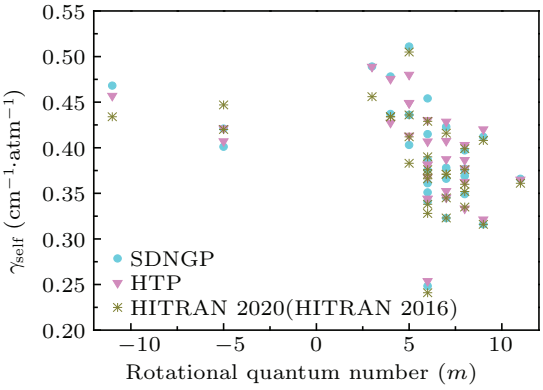



**Fig. 7.** Comparison of the self-broadening coefficients of $H_2{}^{16}O$ lines for different vibrational bands using the SDNGP, the HTP, and reported by the HITRAN database versus rotational quantum number ($m$).

### 3.5. Line narrowing parameters analysis

All the speed-dependent broadening coefficients ($\alpha_W$) fitted with the SDNGP and HTP for our work are given in Fig. 8(a). The average values of $\alpha_W$ obtained with the SDNGP and HTP are 0.051 and 0.092, respectively. Additionally, the ratios of the Dicke narrowing coefficients to the self-broadening coefficients in our work are shown in Fig. 8(b). The average values of $\nu_{VC}/\gamma_{self}$ fitted with the SDNGP and HTP are 0.078 and 0.253, respectively. It is interesting that the values of $\alpha_W$ and $\nu_{VC}/\gamma_{self}$ using the HTP are slightly larger than those using the SDNGP. The outcome indicates that both the Dicke narrowing coefficients and the speed dependent broadening coefficients contribute to the analysis of the spectral line-width.

To check the influence of the Dicke narrowing effect and speed dependent effect on our line-shapes, the values of $\alpha_W/(\nu_{VC}/\gamma_{self})$ obtained with the SDNGP are shown in Fig. 9(a). The result indicates that there is little difference in the narrowing degree of the spectral lines produced by these two effects. Hence, neither of the effects can be ignored and nor can the correlation between them. This result is consistent with the view of Wójtewicz *et al.*[28] that it is difficult to decorrelate the speed dependence of collision broadening and Dicke narrowing. Fig. 9(b) displays the results $\nu_{VC}$ and $\alpha_W$ obtained by HTP as a function of $\eta$. It can be seen from Fig. 9(b) that there seems to be an inverse relationship between the value difference between the two effect-related parameters and the correlation coefficient.

Although the SDNGP and HTP are used to analyze the spectral line parameters in this experiment, we consider what

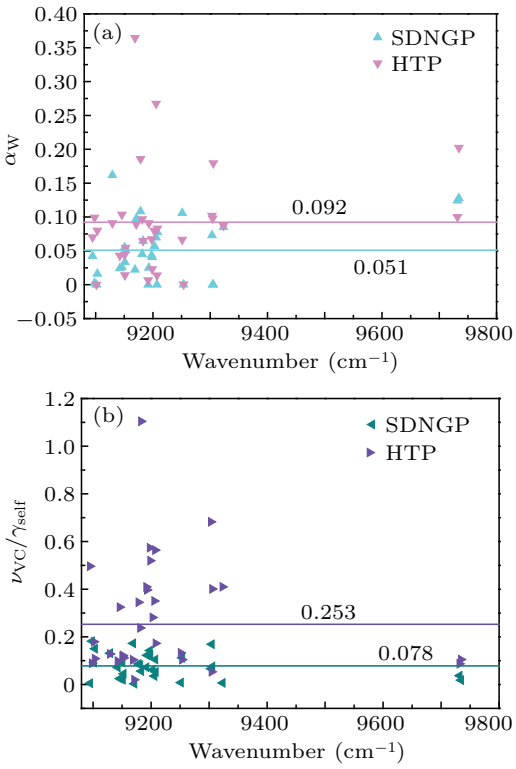



**Fig. 8.** (a) The speed dependent broadening coefficients from SDNGP and HTP fitting. (b) The ratio of Dicke narrowing coefficients and self-broadening coefficients obtained from SDNGP and HTP fitting.

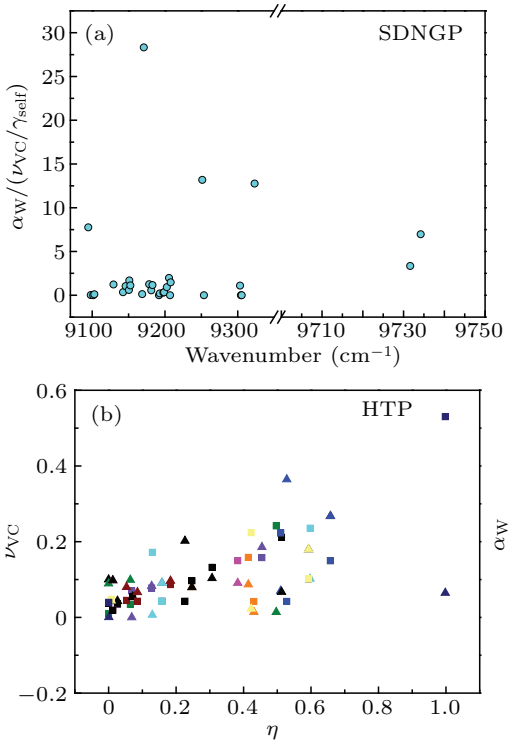



**Fig. 9.** Spectral line narrowing effect parameters. (a) Comparison between $\alpha_W$ and $\nu_{VC}/\gamma_{self}$ obtained by the SDNGP. (b) The relative parameters of the Dicke narrowing effect (square) and the speed dependent effect (triangle) obtained by the HTP.

was mentioned in the literature:[16,29] "Whether the experimental conditions consider an important factor of parameter $\eta$, that is, HTP parameters need to be obtained under the high signal-to-noise ratio spectrum and high precision frequency

standard". In view of the relatively low signal-to-noise ratio (QF $<$ 1000) in our experiment, the spectral line parameters obtained with the SDNGP are more reasonable than those obtained with the HTP.

## 4. Conclusion

We recorded thirty-one absorption spectra of pure water vapor molecules around 1.1 μm. The HTP and SDNGP lineshape models were used to retrieve the spectroscopic parameters from spectral fits. The comparison of the present results with HITRAN 2020 shows that the line intensities of this study for the HTP and SDNGP are smaller than those in HITRAN 2020, with mean differences of $-3.53\%$ and $-3.85\%$. The line intensities obtained by fitting with the HTP and SDNGP are less than those in HITRAN 2016, and the differences between them are $-2.40\%$ and $-2.61\%$. Additionally, the self-broadening coefficients of our work are larger than those of HITRAN 2020 (or HITRAN 2016). The self-broadening coefficients from our HTP- and SDNGP-based work have average percent differences of 3.26% and 2.70% compared with HITRAN 2020 (or HITRAN 2016), respectively. For the line intensities and self-broadening coefficients, preferable agreement is obtained between the present results and the two HITRAN datasets. Therefore, the line parameters obtained in this work are credible. Finally, we discussed the influence of the corresponding parameters of these two effects on the spectral line-width, which has never been reported in the HITRAN database. The spectral line parameters obtained with the SDNGP in this experiment are more reasonable. We believe that the data we obtained will be helpful to the spectral analysis of atmospheric water molecules.

## Acknowledgements

Project supported by the National Natural Science Foundation of China (Grant Nos. 41805014 and 62205005), the Key Program of the Natural Science Research Fund of the Education Department of Anhui Province (Grant Nos. KJ2021A0637 and KJ2021A0638), and the Key Program in the Youth Talent Support Plan in Universities of Anhui Province (Grant No. gxyqZD2020032).

## References

[1] Ibrahim N, Chelin P, Orphal J and Baranov Y I 2008 *J. Quantum Spectrosc. Radiat. Transfer* **109** 2523
[2] Shine K P, Ptashnik I V and Rädel G 2012 *Surv. Geophys.* **33** 535
[3] Wang R W, Xie P H, Xu J and Li A 2019 *Acta Opt. Sin.* **39** 9 (in Chinese)
[4] Goldenstein C S, Spearrin R M, Schultz I A, Jeffries J B and Hanson R K 2014 *Meas. Sci. Tech.* **25** 055101
[5] Zhu W Y, Qian X M, Rao R Z and Wang H 2019 *Infrared and Laser Engineering* **48** 19 (in Chinese) DOI:
[6] Ieg A, Lsr A, Rjh A, *et al.* 2022 *J. Quantum Spectrosc. Radiat. Transfer* **277** 107949
[7] Régalia L, Oudot C, Mikhailenko S, Wang L, Thomas X, Jenouvrier A and Heyden P V 2014 *J. Quantum Spectrosc. Radiat. Transfer* **136** 119
[8] Oudot C, Wang L, Thomas X, Heyden P V D, Daumont L and Régalia L 2010 *J. Mol. Spectros.* **262** 22
[9] Schermaul R, Learner R C M, Newnham D A, Ballard J, Zobov N, Belmiloud D and Tennyson J 2001 *J. Mol. Spectros.* **208** 32
[10] Lance B, Blanquet G, Walrand J and Bouanich J P 1997 *J. Mol. Spectrosc.* **185** 262
[11] Shapiro D A, Ciurylo R, Jaworski R and May A D 2001 *Can. J. Phys.* **79** 1209
[12] Forthomme D, Cich M J, Twagirayezu S, Hall G E and Sears T J 2015 *J. Quantum Spectrosc. Radiat. Transfer* **165** 28
[13] Zheng J J, Ma H L, Liu Q, Qian X M, Zhu W Y, Cao Z S, Chen J, Yang T and Xu Q Y 2022 *Microw. Opt. Technol. Lett.* 1–10 (in Chinese)
[14] Zheng J J, Zhu W Y, Liu Q, Ma H L, Liu K, Qian X M, Chen J and Yang T 2021 *Acta Phys. Sin* **70** 163301 (in Chinese)
[15] Ngo N H, Ibrahim N, Landsheere X, Tran H, Chelin P, Schwell M and Hartmann J M 2012 *J. Quantum Spectrosc. Radiat. Transfer* **113** 870
[16] Adkins E M and Hodges J T 2022 *J. Quantum Spectrosc. Radiat. Transfer* **280** 108100
[17] Schneider M, Hase F, Blavier J F, Toon G C and Leblanc T 2011 *J. Quantum Spectrosc. Radiat. Transfer* **112** 465
[18] Fokin L R and Kalashnikov A N 2008 *High Temp.* **46** 614
[19] Tolchenov R N and Tennyson J 2005 *J. Mol. Spectros.* **231** 23
[20] Ngo N H, Lisak D, Tran H and Hartmann J M 2013 *J. Quantum Spectrosc. Radiat. Transfer* **129** 89
[21] Cygan A, Lisak D, Wójtewicz S, Domysławska J, Hodges J T, Trawiński R S and Ciuryło R 2012 *Phys. Rev. A* **85** 022508
[22] Adkins E M, Long D A, Fleisher A J and Hodges J T 2021 *J. Quantum Spectrosc. Radiat. Transfer* **262** 107527
[23] Moretti L, Sasso A, Gianfrani L and Ciurylo R 2001 *J. Mol. Spectros.* **205** 20
[24] Claveau C, Henry A, Hurtmans D and Valentin A 2001 *J. Quantum Spectrosc. Radiat. Transfer* **68** 273
[25] Wagner G, Birk M, Gamache R R, Gamache R R and Hartmann J M 2005 *J. Quantum Spectrosc. Radiat. Transfer* **92** 211
[26] Long D A, Bielska K, Lisak D, Havey K, Okumura M, Miller C E and Hodges J T 2011 *J. Chem. Phys.* **135** 064308
[27] Li J D, Du Y J, Peng Z M and Ding Y J 2019 *J. Quantum Spectrosc. Radiat. Transfer* **224** 197
[28] Wójtewicz S, Stec K, Masłowski P, Cygan A, Lisak D, Trawiński R S and Ciuryło R 2013 *J. Quantum Spectrosc. Radiat. Transfer* **130** 191
[29] Fleurbaey H, Reed Z D, Adkins E M, Long D A and Hodges J T 2021 *J. Quantum Spectrosc. Radiat. Transfer* **270** 107684